Chapter 10

Pulse Characterization

Characterization of ultrashort laser pulses with pulse widths greater than 20 ps can be directly performed electronically using high speed photo detectors and sampling scopes. Photo detectors with bandwidth of 100 GHz are available. For shorter pulses usually some type of autocorrelation or cross-correlation in the optical domain using nonlinear optical effects has to be performed, i.e. the pulse itself has to be used to measure its width, because there are no other controllable events available on such short time scales.

10.1   Intensity Autocorrelation

Pulse duration measurements using second-harmonic intensity autocorrelation is a standard method for pulse characterisation. Figure 10.1 shows the setup for a background free intensity autocorrelation. The input pulse is split in two, and one of the pulses is delayed by τ. The two pulses are focussed into a nonliner optical crystal in a non-colinear fashion. The nonlinear optical crystal is designed for efficient second harmonic generation over the full bandwidth of the pulse, i.e. it has a large second order nonlinear optical suszeptibility and is phase matched for the specific wavelength range. We do not consider the z–dependence of the electric field and phase–matching effects. To simplify notation, we omit normalization factors. The induced nonlinear polarization is expressed as a convolution of two interfering electric–fields $E_1(t)$, $E_2(t)$ with the nonlinear response function of the medium, the

second order nonlinear susceptibility $\chi^{(2)}$.

$$P^{(2)}(t) \propto \iint_{-\infty}^{\infty} \chi^{(2)}(t - t_1, t - t_2) \cdot E_1(t_1) \cdot E_2(t_2) dt_1 dt_2$$

Image removed due to copyright restrictions.

Please see:

Keller, U., Ultrafast Laser Physics, Institute of Quantum Electronics, Swiss Federal Institute of Technology, ETH Hönggerberg—HPT, CH-8093 Zurich, Switzerland.

Figure 10.1: Setup for a background free intensity autocorrelation. To avoid dispersion and pulse distortions in the autocorrelator reflective optics can be and a thin crystal has to be used for measureing very short, typically sub-100 fs pulses.

We assume the material response is instantaneous and replace $\chi^{(2)}(t - t_1, t - t_2)$ by a Dirac delta–function $\chi^{(2)} \cdot \delta(t - t_1) \cdot \delta(t - t_2)$ which leads to

$$P^{(2)}(t) \propto E_1(t) \cdot E_2(t) \tag{10.1}$$

Due to momentum conservation, see Figure 10.1, we mayseparate the product $E(t) \cdot E(t - \tau)$ geometrically and supress a possible background coming from simple SHG of the individual pulses alone. The signal is zero if the pulses don't overlap.

$$P^{(2)}(t) \propto E(t) \cdot E(t - \tau). \tag{10.2}$$

Table 10.1: Pulse shapes and its deconvolution factors relating FWHM, τ_p, of the pulse to FWHM, τ_A, of the intensity autocorrelationfunction.

The electric field of the second harmonic radiation is directly proportional to the polarization, assuming a nondepleted fundamental radiation and the use of thin crystals. Due to momentum conservation, see Figure 10.1, we find

$$I_{AC}(\tau) \quad \propto \quad \int_{-\infty}^{\infty} \left| A(t)A(t-\tau) \right|^2 dt. \qquad (10.3)$$

$$\propto \quad \int_{-\infty}^{\infty} I(t)I(t-\tau)\ dt, \qquad (10.4)$$

with the complex envelope $A(t)$ and intensity $I(t) = |A(t)|^2$ of the input pulse. The photo detector integrates because its response is usually much slower than the pulsewidth. Note, that the intenisty autocorrelation is symmetric by construction

$$I_{AC}(\tau) = I_{AC}(-\tau). \tag{10.5}$$

It is obvious from Eq.(10.3) that the intensity autocorrelation does not contain full information about the electric field of the pulse, since the phase of the pulse in the time domain is completely lost. However, if the pulse shape is known the pulse width can be extracted by deconvolution of the correlation function. Table 10.1 gives the deconvolution factors for some often used pulse shapes.

10.2   Interferometric Autocorrelation (IAC)

A pulse characterization method, that also reveals the phase of the pulse is the interferometric autocorrelation introduced by J. C. Diels [2], (Figure 10.2 a). The input beam is again split into two and one of them is delayed. However, now the two pulses are sent colinearly into the nonlinear crystal. Only the SHG component is detected after the filter.

Image removed due to copyright restrictions.

Please see:

Keller, U., Ultrafast Laser Physics, Institute of Quantum Electronics, Swiss Federal Institute of Technology, ETH Hönggerberg—HPT, CH-8093 Zurich, Switzerland.

Figure 10.2: (a) Setup for an interferometric autocorrelation. (b) Delay stage, so that both beams are reflected from the same air/medium interface imposing the same phase shifts on both pulses.

The total field $E(t, \tau)$ after the Michelson-Interferometer is given by the two identical pulses delayed by τ with respect to each other

$$
\begin{aligned}
E(t, \tau) &= E(t + \tau) + E(t) & (10.6)\\
&= A(t + \tau)e^{j\omega_C(t+\tau)}e^{j\phi_{CE}} + A(t)e^{j\omega_c t}e^{j\phi_{CE}} . & (10.7)
\end{aligned}
$$

$A(t)$ is the complex amplitude, the term $e^{i\omega_0 t}$ describes the oscillation with the carrier frequency ω_0 and ϕ_{CE} is the carrier-envelope phase. Eq. (10.1) writes

$$
P^{(2)}(t, \tau) \propto \left(A(t + \tau)e^{j\omega_c(t+\tau)}e^{j\phi_{CE}} + A(t)e^{j\omega_c t}e^{j\phi_{CE}} \right)^2 \qquad (10.8)
$$

This is only idealy the case if the paths for both beams are identical. If for example dielectric or metal beamsplitters are used, there are different reflections involved in the Michelson-Interferometer shown in Fig. 10.2 (a) leading to a differential phase shift between the two pulses. This can be avoided by an exactly symmetric delay stage as shown in Fig. 10.1 (b).

Again, the radiated second harmonic electric field is proportional to the polarization

$$
E(t, \tau) \propto \left(A(t + \tau)e^{j\omega_c(t+\tau)}e^{j\phi_{CE}} + A(t)e^{j\omega_c(t)}e^{j\phi_{CE}} \right)^2 . \qquad (10.9)
$$

The photo–detector (or photomultiplier) integrates over the envelope of each individual pulse

$$
\begin{aligned}
I(\tau) \ &\propto \ \int_{-\infty}^{\infty} \left| \left(A(t + \tau)e^{j\omega_c(t+\tau)} + A(t)e^{j\omega_c t} \right)^2 \right|^2 dt . \\
&\propto \ \int_{-\infty}^{\infty} \Big| A^2(t + \tau)e^{j2\omega_c(t+\tau)} \\
&\qquad\qquad + 2A(t + \tau)A(t)e^{j\omega_c(t+\tau)}e^{j\omega_c t} \\
&\qquad\qquad + A^2(t)e^{j2\omega_c t} \Big|^2 . \qquad (10.10)
\end{aligned}
$$

Evaluation of the absolute square leads to the following expression

$$
\begin{aligned}
I(\tau) \ \propto \ \int_{-\infty}^{\infty} \Big[&|A(t + \tau)|^4 + 4|A(t + \tau)|^2|A(t)|^2 + |A(t)|^4 \\
&+ 2A(t + \tau)|A(t)|^2 A^*(t)e^{j\omega_c \tau} + \text{c.c.} \\
&+ 2A(t)|A(t + \tau)|^2 A^*(t + \tau)e^{-j\omega_c \tau} + \text{c.c.} \\
&+ A^2(t + \tau)(A^*(t))^2 e^{j2\omega_c \tau} + \text{c.c.} \Big] dt . \qquad (10.11)
\end{aligned}
$$

The carrier–envelope phase ϕ_{CE} drops out since it is identical to both pulses. The interferometric autocorrelation function is composed of the following terms

$$I(\tau) = I_{back} + I_{int}(\tau) + I_{\omega}(\tau) + I_{2\omega}(\tau) \ . \tag{10.12}$$

Background signal I_{back}:

$$I_{back} = \int_{-\infty}^{\infty} \left(|A(t+\tau)|^4 + |A(t)|^4 \right) \, dt = 2 \int_{-\infty}^{\infty} I^2(t) \, dt \tag{10.13}$$

Intensity autocorrelation $I_{int}(\tau)$:

$$I_{int}(\tau) = 4 \int_{-\infty}^{\infty} |A(t+\tau)|^2 |A(t)|^2 \, dt = 4 \int_{-\infty}^{\infty} I(t+\tau) \cdot I(t) \, dt \tag{10.14}$$

Coherence term oscillating with ω_c: $I_{\omega}(\tau)$:

$$I_{\omega}(\tau) = 4 \int_{-\infty}^{\infty} \mathrm{Re}\left[\left(I(t) + I(t+\tau) \right) A^*(t) A(t+\tau) e^{j\omega\tau} \right] dt \tag{10.15}$$

Coherence term oscillating with $2\omega_c$: $I_{2\omega}(\tau)$:

$$I_{\omega}(\tau) = 2 \int_{-\infty}^{\infty} \mathrm{Re}\left[A^2(t)(A^*(t+\tau))^2 e^{j2\omega\tau} \right] dt \tag{10.16}$$

Eq. (10.12) is often normalized relative to the background intensity I_{back} resulting in the interferometric autocorrelation trace

$$I_{IAC}(\tau) = 1 + \frac{I_{int}(\tau)}{I_{back}} + \frac{I_{\omega}(\tau)}{I_{back}} + \frac{I_{2\omega}(\tau)}{I_{back}}. \tag{10.17}$$

Eq. (10.17) is the final equation for the normalized interferometric autocorrelation. The term $I_{int}(\tau)$ is the intensity autocorrelation, measured by non–colinear second harmonic generation as discussed before. Therefore, the averaged interferometric autocorrelation results in the intensity autocorrelation sitting on a background of 1.

Fig. 10.3 shows a calculated and measured IAC for a sech-shaped pulse.

Image removed due to copyright restrictions.

Please see:

Keller, U., Ultrafast Laser Physics, Institute of Quantum Electronics, Swiss Federal Institute of Technology, ETH Hönggerberg—HPT, CH-8093 Zurich, Switzerland.

Figure 10.3: Computed and measured interferometric autocorrelation traces for a 10 fs long sech-shaped pulse.

As with the intensity autorcorrelation, by construction the interferometric autocorrelation has to be also symmetric:

$$I_{IAC}(\tau) = I_{IAC}(-\tau) \tag{10.18}$$

This is only true if the beam path between the two replicas in the setup are completely identical, i.e. there is not even a phase shift between the two pulses. A phase shift would lead to a shift in the fringe pattern, which shows up very strongly in few-cycle long pulses. To avoid such a symmetry breaking, one has to arrange the delay line as shown in Figure 10.2 b so that each pulse travels through the same amount of substrate material and undergoes the same reflections.

At $\tau = 0$, all integrals are identical

$$I_{back} \equiv 2 \int |A(t)|^4 dt$$

$$I_{int}(\tau = 0) \equiv 2 \int |A^2(t)|^2 dt = 2 \int |A(t)|^4 dt = I_{back}$$

$$I_\omega(\tau = 0) \equiv 2 \int |A(t)|^2 A(t) A^*(t) dt = 2 \int |A(t)|^4 dt = I_{back}$$

$$I_{2\omega}(\tau = 0) \equiv 2 \int A^2(t)(A^2(t)^* dt = 2 \int |A(t)|^4 dt = I_{back}$$

$$(10.19)$$

Then, we obtain for the interferometric autocorrelation at zero time delay

$$I_{IAC}(\tau)|_{\max} = I_{IAC}(0) = 8$$

$$I_{IAC}(\tau \to \pm\infty) = 1 \tag{10.20}$$

$$I_{IAC}(\tau)|_{\min} = 0$$

This is the important 1:8 ratio between the wings and the pick of the IAC, which is a good guide for proper alignment of an interferometric autocorrelator. For a chirped pulse the envelope is not any longer real. A chirp in the pulse results in nodes in the IAC. Figure 10.4 shows the IAC of a chirped sech-pulse

$$A(t) = \left(\text{sech} \left(\frac{t}{\tau_p} \right) \right)^{(1+j\beta)}$$

for different chirps.

Image removed due to copyright restrictions.

Please see:
Keller, U., Ultrafast Laser Physics, Institute of Quantum Electronics, Swiss Federal Institute of Technology,
ETH Hönggerberg—HPT, CH-8093 Zurich, Switzerland.

Figure 10.4: Influence of increasing chirp on the IAC.

10.2.1 Interferometric Autocorrelation of an Unchirped Sech-Pulse

Envelope of an unchirped sech-pulse

$$A(t) = \mathrm{sech}(t/\tau_p) \tag{10.21}$$

Interferometric autocorrelation of a sech-pulse

$$
\begin{aligned}
I_{IAC}(\tau) =\ & 1 + \{2 + \cos(2\omega_c\tau)\} \frac{3\left(\left(\frac{\tau}{\tau_p}\right)\cosh\left(\frac{\tau}{\tau_p}\right) - \sinh\left(\frac{\tau}{\tau_p}\right)\right)}{\sinh^3\left(\frac{\tau}{\tau_p}\right)} \\
& + \frac{3\left(\sinh\left(\frac{2\tau}{\tau_p}\right) - \left(\frac{2\tau}{\tau_p}\right)\right)}{\sinh^3\left(\frac{\tau}{\tau_p}\right)} \cos(\omega_c\tau)
\end{aligned}
\tag{10.22}
$$

10.2.2   Interferometric Autocorrelation of a Chirped Gaussian Pulse

Complex envelope of a Gaussian pulse

$$A(t) = \exp\left[-\frac{1}{2}\left(\frac{t}{t_p}\right)(1+j\beta)\right]. \tag{10.23}$$

Interferometric autocorrelation of a Gaussian pulse

$$
\begin{aligned}
I_{IAC}(\tau) \;=\; & 1 + \left\{2 + e^{-\frac{\beta^2}{2}\left(\frac{\tau}{\tau_p}\right)^2}\cos(2\omega_c\tau)\right\}e^{-\frac{1}{2}\left(\frac{\tau}{\tau_p}\right)^2} \\
& + 4e^{-\frac{3+\beta^2}{8}\left(\frac{\tau}{\tau_p}\right)^2}\cos\left(\frac{\beta}{4}\left(\frac{\tau}{\tau_p}\right)^2\right)\cos\left(\omega_c\tau\right).
\end{aligned}
\tag{10.24}
$$

10.2.3   Second Order Dispersion

It is fairly simple to compute in the Fourier domain what happens in the presence of dispersion.

$$E(t) = A(t)e^{j\omega_c t} \xrightarrow{F} \tilde{E}(\omega) \tag{10.25}$$

After propagation through a dispersive medium we obtain in the Fourier domain.

$$\tilde{E}'(\omega) = \tilde{E}(\omega)e^{-i\Phi(\omega)}$$

and

$$E'(t) = A'(t)e^{j\omega_c t}$$

Figure 10.5 shows the pulse amplitude before and after propagation through a medium with second order dispersion. The pulse broadens due to the dispersion. If the dispersion is further increased the broadening increases and the interferometric autocorrelation traces shown in Figure 10.5 develope a characteristic pedestal due to the term I_{int}. The width of the interferometrically sensitive part remains the same and is more related to the coherence time in the pulse, that is proportional to the inverse spectral width and does not change.

Figure 10.5: Effect of various amounts of second order dispersion on a transform limited 10 fs Sech-pulse.

10.2.4 Third Order Dispersion

We expect, that third order dispersion affects the pulse significantly for

$$\frac{D_3}{\tau^3} > 1$$

which is for a 10fs sech-pulse $D_3 > \left(\frac{10 \text{ fs}}{1.76}\right)^3 \approx 183 \text{ fs}^3$. Figure 10.6 and 10.7 show the impact on pulse shape and interferometric autocorrelation. The odd dispersion term generates asymmetry in the pulse. The interferometric autocorrelation developes characteristic nodes in the wings.

Image removed due to copyright restrictions.

Please see:

Keller, U., Ultrafast Laser Physics, Institute of Quantum Electronics, Swiss Federal Institute of Technology, ETH Hönggerberg—HPT, CH-8093 Zurich, Switzerland.

Figure 10.6: Impact of 200 fs^3 third order dispersion on a 10 fs pulse at a center wavelength of 800 nm.and its interferometric autocorrelation.

Image removed due to copyright restrictions.

Please see:

Keller, U., Ultrafast Laser Physics, Institute of Quantum Electronics, Swiss Federal Institute of Technology, ETH Hönggerberg—HPT, CH-8093 Zurich, Switzerland.

Figure 10.7: Changes due to increasing third order Dispersion from 100-1000 fs^{3}on a 10 fs pulse at a center wavelength of 800 nm.

10.2.5 Self-Phase Modulation

Self-phase modulation without compensation by proper negative dispersion generates a phase over the pulse in the time domain. This phase is invisible in the intensity autocorrelation, however it shows up clearly in the IAC, see Figure 10.8 for a Gaussian pulse with a peak nonlinear phase shift $\phi_0 = \delta A_0^2 = 2$ and Figure 10.8 for a nonlinear phase shift $\phi_0 = 3$.

Image removed due to copyright restrictions.

Please see:

Keller, U., Ultrafast Laser Physics, Institute of Quantum Electronics, Swiss Federal Institute of Technology, ETH Hönggerberg—HPT, CH-8093 Zurich, Switzerland.

Figure 10.8: Change in pulse shape and interferometric autocorrelation in a 10 fs pulse at 800 nm subject to pure self-phase modulation leading to a nonlinear phase shift of $\phi_0 = 2$.

Image removed due to copyright restrictions.

Please see:

Keller, U., Ultrafast Laser Physics, Institute of Quantum Electronics, Swiss Federal Institute of Technology, ETH Hönggerberg—HPT, CH-8093 Zurich, Switzerland.

Figure 10.9: Change in pulse shape and interferometric autocorrelation in a 10 fs pulse at 800 nm subject to pure self-phase modulation leading to a nonlinear phase shift of $\phi_0 = 3$.

From the expierence gained by looking at the above IAC-traces for pulses undergoing second and third order dispersions as well as self-phase modulation we conclude that it is in general impossible to predict purely by looking at the IAC what phase perturbations a pulse might have. Therefore, it was always a wish to reconstruct uniquely the electrical field with respect to amplitude and phase from the measured data. In fact one can show rigorously, that amplitude and phase of a pulse can be derived uniquely from the IAC and the measured spectrum up to a time reversal ambiguityn [1]. Furthermore, it has been shown that a cross-correlation of the pulse with a replica

chirped in a known medium and the pulse spectrum is enough to reconstruct the pulse [3]. Since the spectrum of the pulse is already given only the phase has to be determined. If a certain phase is assumed, the electric field and the measured cross-correlation or IAC can be computed. Minimization of the error between the measured cross-correlation or IAC will give the desired spectral phase. This procedure has been dubbed PICASO (Phase and Intenisty from Cross Correlation and Spectrum Only).

Note, also instead of measuring the autocorrelation and interferometric autocorrelation with SHG one can also use two-photon absorption or higher order absorption in a semiconductor material (Laser or LED) [4].

However today, the two widely used pulse chracterization techniques are Frequency Resolved Optical Gating (FROG) and Spectral Phase Interferometry for Direct Electric Field Reconstruction (SPIDER)

10.3 Frequency Resolved Optical Gating (FROG)

We follow closely the bock of the FROG inventor Rich Trebino. In frequency resolved optical gating, the pulse to be characterized is gated by another ultrashort pulse [5]. The gating is no simple linear sampling technique, but the pulses are crossed in a medium with an instantaneous nonlinearity ($\chi^{(2)}$ or $\chi^{(3)}$) in the same way as in an autocorrelation measurement (Figures 10.1 and 10.10). The FROG–signal is a convolution of the unknown electric–field $E(t)$ with the gating–field $g(t)$ (often a copy of the unknown pulse itself). However, after the interaction of the pulse to be measured and the gate pulse, the emitted nonlinear optical radiation is not put into a simple photo detector, but is instead spectrally resolved detected. The general form of the frequency–resolved intensity, or Spectrogram $S_F(\tau, \omega)$ is given by

$$S_F(\tau, \omega) \propto \left| \int_{-\infty}^{\infty} E(t) \cdot g(t - \tau) e^{-j\omega t} dt \right|^2 . \qquad (10.26)$$

Image removed due to copyright considerations.

Figure 10.10: The spectrogram of a waveform E(t) tells the intensity and frequency in a given time interval [5].

Representations of signals, or waveforms in general, by time-frequency distributions has a long history. Most notabley musical scores are a temporal sequence of tones giving its frequency and volume, see Fig. 10.11.
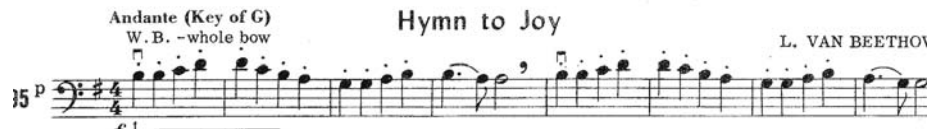

Figure 10.11: A musical score is a time-frequency representation of the signal to be played.

Time-frequency representations are well known in the radar community, signal processing and quantum mechanics [9] (Spectrogram, Wigner-Distribution, Husimi-Distribution, ...), Figure 10.12 shows the spectrogram of differently chirped pulses. Like a mucical score, the spectrogram visually displays the frequency vs. time.

Image removed due to copyright considerations.

Figure 10.12: Like a musical score, the spectrogram visually displays the frequency vs. time [5].

Note, that the gate pulse in the FROG measurement technique does not to be very short. In fact if we have

$$g(t) \equiv \delta(t) \tag{10.27}$$

then

$$S_F(\tau, \omega) = |E(\tau)|^2 \tag{10.28}$$

and the phase information is completely lost. There is no need for short gate pulses. A gate length of the order of the pulse length is sufficient. It temporally resolves the slow components and spectrally the fast components.

10.3.1 Polarization Gate FROG

Figure 10.13 shows the setup [6][7]. FROG is based on the generation of a well defined gate pulse, eventually not yet known. This can be achieved by using the pulse to be measured and an ultrafast nonlinear interaction. For example the electronic Kerr effect can be used to induce an ultrafast polarization modulation, that can gate the pulse with a copy of the same pulse.
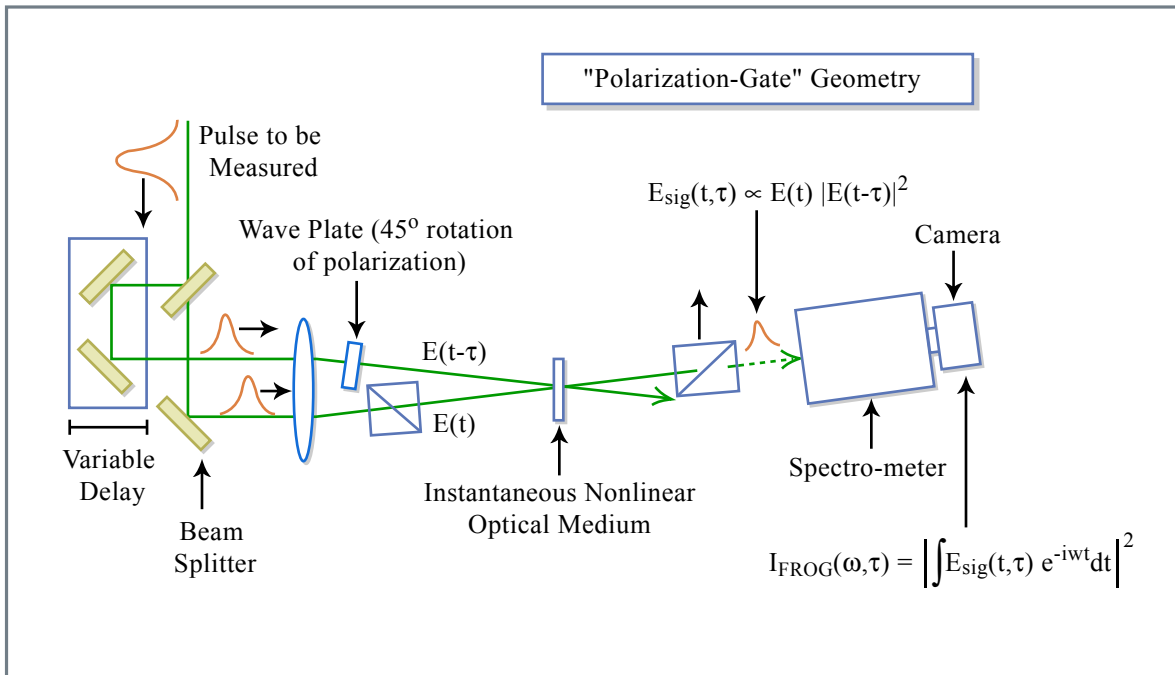
"Polarization-Gate" Geometry

Pulse to be Measured

Wave Plate (45° rotation of polarization)

$E_{sig}(t,\tau) \propto E(t) |E(t-\tau)|^2$

Camera

$E(t-\tau)$

$E(t)$

Variable Delay

Beam Splitter

Instantaneous Nonlinear Optical Medium

Spectro-meter

$I_{FROG}(\omega,\tau) = \left| \int E_{sig}(t,\tau) \, e^{-iwt} dt \right|^2$

Figure 10.13: Polarization Gate FROG setup. The instantaneous Kerr-effect is used to rotate the polarization of the signal pulse $E(t)$ during the presence of the gate pulse $E(t - \tau)$ proportional to the intensity of the gate pulse [5].

Figure by MIT OCW.

The signal analyzed in the FROG trace is, see Figure 10.14,

$$E_{sig}(t, \tau) = E(t) |E(t - \tau)|^2 \qquad (10.29)$$

Image removed due to copyright considerations.

Figure 10.14: The signal pulse reflects the color of the gated pulse at the time $2\tau/3$ [5]

The FROG traces generated from a PG-FROG for chirped pulses is identical to Fig. 10.12. Figure 10.15 shows FROG traces of more complicated pulses

Image removed due to copyright considerations.

Figure 10.15: FROG traces of more complicated pulses.

10.3.2   FROG Inversion Algorithm

Spectrogram inversion algorithms need to know the gate function $g(t - \tau)$, which in the given case is related to the yet unknown pulse. So how do we get from the FROG trace to the pulse shape with respect to amplitude and phase? If there is such an algorithm, which produces solutions, the question of uniquness of this solution arises. To get insight into these issues, we realize, that the FROG trace can be written as

$$I_{FROG}(\tau, \omega) \propto \left| \int_{-\infty}^{\infty} E_{sig}(t, \tau) e^{-j\omega t} dt \right|^2 \qquad (10.30)$$

Writing the signal field as a Fourier transform in the time variable, i.e.

$$E_{sig}(t, \tau) = \int_{-\infty}^{\infty} \hat{E}_{sig}(t, \Omega) e^{-j\Omega \tau} d\Omega \qquad (10.31)$$

yields

$$I_{FROG}(\tau,\omega) \propto \left| \int_{-\infty}^{\infty} \int_{-\infty}^{\infty} \hat{E}_{sig}(t,\Omega) e^{-j\omega t - j\Omega\tau} dt d\Omega \right|^2 . \qquad (10.32)$$

This equation shows that the FROG-trace is the magnitude square of a two-dimensional Fourier transform related to the signal field $E_{sig}(t,\tau)$. The inversion of Eq.(10.32) is known as the 2D-phase retrieval problem. Fortunately algorithms for this inversion exist [8] and it is known that the magnitude (or magnitude square) of a 2D-Fourier transform (FT) essentially uniquely determines also its phase, if additional conditions, such as finite support or the relationship (10.29) is given. Essentially unique means, that there are ambiguities but they are not dense in the function space of possible 2D-transforms, i.e. they have probability zero to occur.

Furthermore, the unknown pulse $E(t)$ can be easily obtained from the modified signal field $\hat{E}_{sig}(t,\Omega)$ because

$$\hat{E}_{sig}(t,\Omega) = \int_{-\infty}^{\infty} E_{sig}(t,\tau) e^{j\Omega\tau} d\tau \qquad (10.33)$$

$$= \int_{-\infty}^{\infty} E(t)g(t-\tau) e^{-j\Omega\tau} d\tau \qquad (10.34)$$

$$= E(t)G^*(\Omega) e^{-j\Omega t} \qquad (10.35)$$

with

$$G(\Omega) = \int_{-\infty}^{\infty} g(\tau) e^{-j\Omega\tau} d\tau. \qquad (10.36)$$

Thus there is

$$E(t) \propto \hat{E}_{sig}(t,0). \qquad (10.37)$$

The only condition is that the gate function should be chosen such that $G(\Omega) \neq 0$. This is very powerful.

Fourier Transform Algorithm

The Fourier transform algorithm also commonly used in other phase retrieval problems is schematically shown in Fig. 10.16
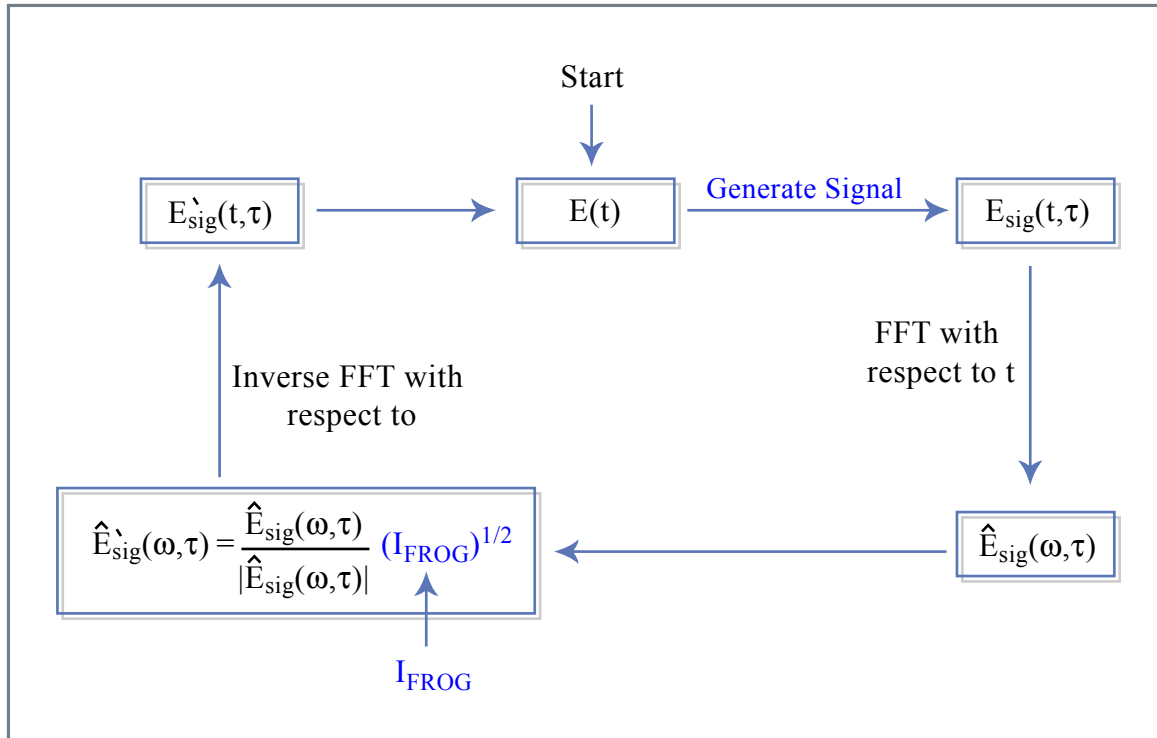
Start

$E`_{sig}(t,\tau)$ $\xrightarrow{}$ $E(t)$ $\xrightarrow{\text{Generate Signal}}$ $E_{sig}(t,\tau)$

FFT with
respect to t

Inverse FFT with
respect to

$\hat{E}`_{sig}(\omega,\tau) = \dfrac{\hat{E}_{sig}(\omega,\tau)}{|\hat{E}_{sig}(\omega,\tau)|}(I_{FROG})^{1/2}$ $\xleftarrow{}$ $\hat{E}_{sig}(\omega,\tau)$

I_{FROG}

Figure 10.16: Fourier transform algorithm for FROG trace inversion. The blue operations indicate the constraints due to the gating technique used and the FROG data [5]

Figure by MIT OCW.

Generalized Projections

The signal field $E_{sig}(t, \tau)$ has to fulfill two constraints, which define sets see Fig. 10.17. The intersection between both sets results in yields $E(t)$. Moving to the closest point in one constraint set and then the other yields convergence to the solution, if the two sets or convex. Unfortunately, the FROG constraints are not convex. Nevertheless the algorithm works surprisingly well. For more information consult with reference [5].
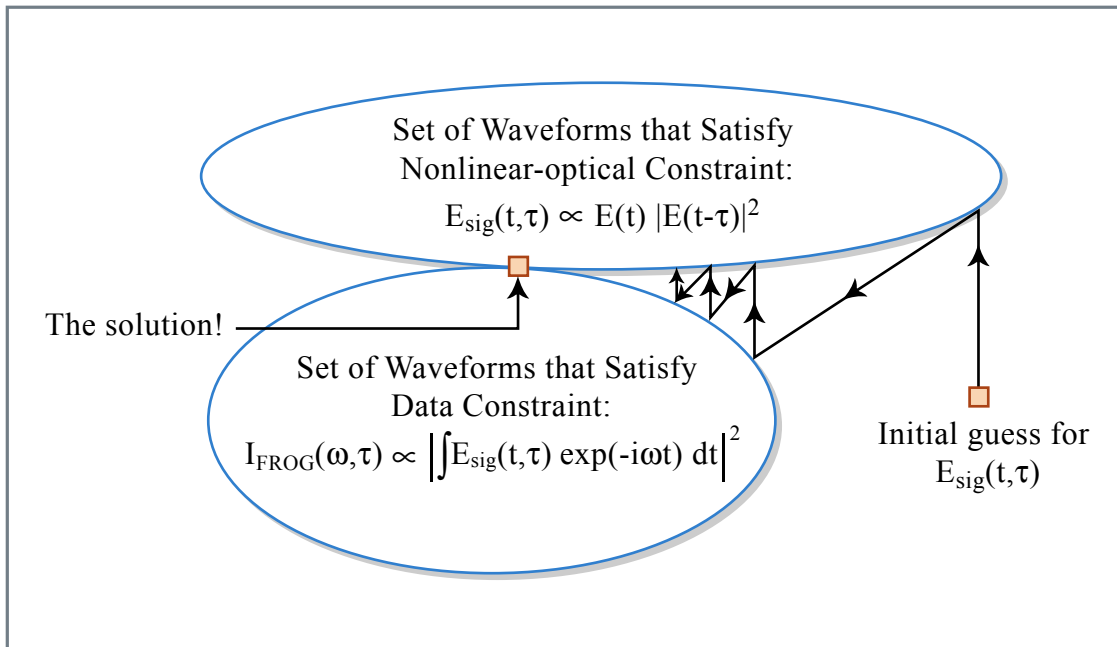
Set of Waveforms that Satisfy
Nonlinear-optical Constraint:

$E_{sig}(t,\tau) \propto E(t) |E(t-\tau)|^2$

The solution!

Set of Waveforms that Satisfy
Data Constraint:

$I_{FROG}(\omega,\tau) \propto \left|\int E_{sig}(t,\tau) \exp(-i\omega t) \, dt\right|^2$

Initial guess for
$E_{sig}(t,\tau)$

Figure 10.17: Generalized Projections applied to FROG [5].

Figure by MIT OCW.

10.3.3   Second Harmonic FROG

So far we only discussed PG-FROG. However, if we choose a $\chi^{(2)}$ nonlinearity, e.g. SHG, and set the gating–field equal to a copy of the pulse $g(t) \equiv E(t)$, we are measuring in eq.(10.26) the spectrally resolved autocorrelation signal. The marginals of the measured FROG-trace do have the following properties

$$\int_{-\infty}^{\infty} S_F(\tau, \omega)\, d\omega \propto \int_{-\infty}^{\infty} |E(t)|^2 \cdot |g(t - \tau)|^2\, dt = I_{AC}(\tau). \qquad (10.38)$$

$$\int_{-\infty}^{\infty} S_F(\tau, \omega)\, d\tau \propto \left| \int_{-\infty}^{\infty} \hat{E}(\omega) \cdot \hat{G}(\omega - \omega')^2 d\omega' \right| = \left| \hat{E}_{2\omega}(\omega) \right|^2. \qquad (10.39)$$

For the case, where $g(t) \equiv E(t)$, we obtain

$$\int_{-\infty}^{\infty} S_F(\tau, \omega)\, d\omega \propto I_{AC}(\tau). \qquad (10.40)$$

$$\int_{-\infty}^{\infty} S_F(\tau, \omega)\, d\tau \propto \left| \hat{E}_{2\omega}(\omega) \right|^2. \qquad (10.41)$$

The setup to measure the Frog-trace is identical with the setup to measure the intensity autocorrelation function (Figure 10.1) only the photodector for the second harmonic is replaced by a spectrometer (Figure 10.18).
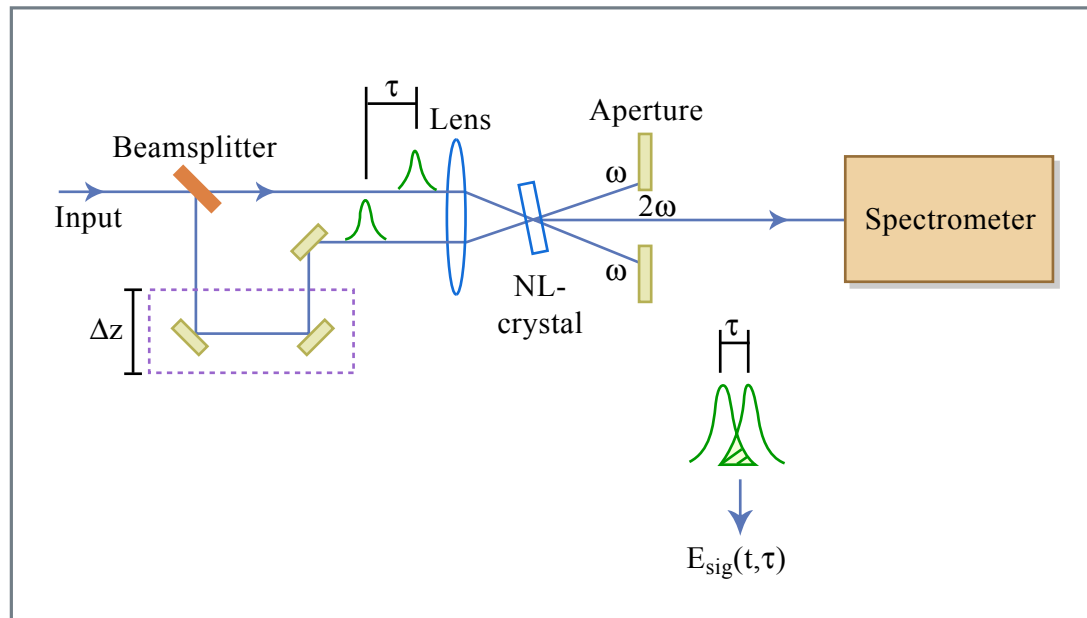

Figure 10.18: SHG-FROG setup.

Figure by MIT OCW.

Since the intensity autocorrelation function and the integrated spectrum can be measured simultaneously, this gives redundancy to check the correctness of all measurements via the marginals (10.38, 10.39). Figure 10.19 shows the SHG-FROG trace of the shortest pulses measured sofar with FROG.
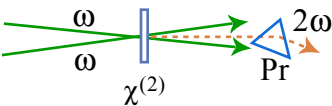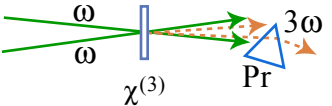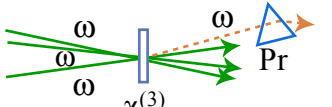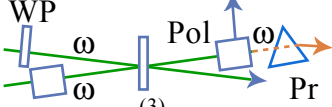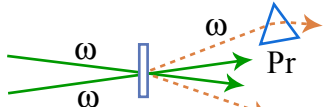
Image removed due to copyright restrictions.

Please see:

Baltuska, Pshenichnikov, and Wiersma. *Journal of Quantum Electronics* 35 (1999): 459.

Figure 10.19: FROG measurement of a 4.5 fs laser pulse.

10.3.4   FROG Geometries

The Frog-signal E_{sig}.can also be generated by a nonlinear interaction different from SHG or PG, see table 10.20[5].

FROG Geometries: Pros and Cons			
	Sensitivity	Ambiguities	
SHG	.001 nJ	Direction of time; Rel. phase of multiple pulses	Most sensitive; most accurate
THG	1 nJ	Relative phase of multiple pulses	Tightly focused beams
TG	10 nJ	None	Useful for UV and transient-grating experiments
PG	100 nJ	None	Simple, intuitive, best scheme for amplified pulses
SD	1000 nJ	None	Useful for UV

SHG = Second-harmonic generation   THG = Third-harmonic generation   TG = Transient-grating

PG = Polarization-gate   SD = Self-diffraction

Figure 10.20: FROG geometries and their pros and cons.

Figure by MIT OCW.

10.4 Spectral Interferometry and SPIDER

Spectral Phase Interferometry for Direct Electric–Field Reconstruction (SPI-DER) avoids iterative reconstruction of the phase profile. Iterative Fourier transform algorithms do have the disadvantage of sometimes being rather time consuming, preventing real–time pulse characterization. In addition, for "pathological" pulse forms, reconstruction is difficult or even impossible. It is mathematically not proven that the retrieval algorithms are unambiguous especially in the presence of noise.

Spectral shearing interferometry provides an elegant method to overcome these disadvantages. This technique has been first introduced by C. Iaconis and I.A. Walmsley in 1999 [11] and called spectral phase interferometry for direct electric–field reconstruction – SPIDER. Before we discuss SPIDER lets look at spectral interferometry in general

10.4.1 Spectral Interferometry

The spectrum of a pulse can easily be measured with a spectrometer. The pulse would be completely know, if we could determine the phase across the spectrum. To determine this unknown phase spectral interferometry for pulse measurement has been proposed early on by Froehly and others [12]. If we would have a well referenced pulse with field $E_R(t)$, superimpose the unknown electric field $E_S(t)$ delayed with the reference pulse and interfere them in a spectrometer, see Figure 10.21, we obtain for the spectrometer output

$$
\begin{aligned}
E_I(t) &= E_R(t) + E_S(t - \tau) & (10.42) \\
\hat{S}(\omega) &= \left| \int_{-\infty}^{+\infty} E_I(t) e^{-j\omega t} dt \right|^2 = \left| \hat{E}_R(\omega) + \hat{E}_S(\omega)^{-j\omega\tau} \right|^2 & (10.43) \\
&= \hat{S}_{DC}(\omega) + \hat{S}^{(-)}(\omega) e^{j\omega\tau} + \hat{S}^{(+)}(\omega) e^{-j\omega\tau} & (10.44)
\end{aligned}
$$

with

$$
\begin{aligned}
\hat{S}^{(+)}(\omega) &= \hat{E}_R^*(\omega) \hat{E}_S(\omega) & (10.45) \\
\hat{S}^{(-)}(\omega) &= \hat{S}^{(+)*}(\omega) & (10.46)
\end{aligned}
$$

Where (+) and (-) indicate as before, well separted positive and negative "frequency" signals, where "frequency" is now related to τ rather than ω.
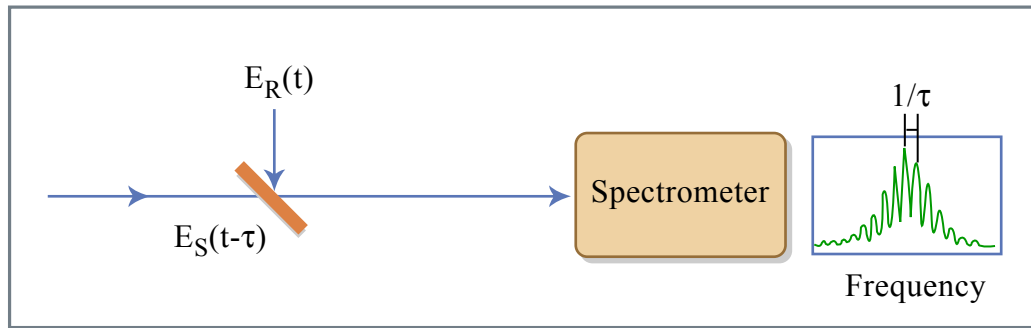
Figure 10.21: Spectral Interferometery of a signal pulse with a reference pulse.

Figure by MIT OCW.

If τ is chosen large enough, the inverse Fourier transformed spectrum $S(t) = F^{-1}\{\hat{S}(\omega)\}$ results in well separated signals, see Figure 10.22.

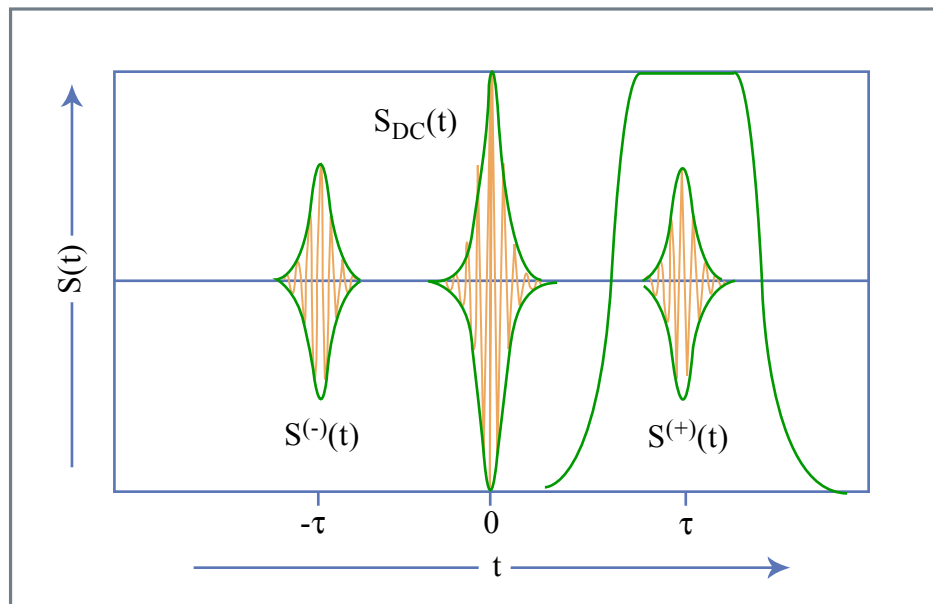$$S(t) = S_{DC}(t) + S^{(-)}(t+\tau) + \hat{S}^{(+)}(t-\tau) \tag{10.47}$$

Figure 10.22: Decomposition of SPIDER signal.

Figure by MIT OCW.

We can isolate either the positive or negative frequency term with a filter in the time domain. Back transformation of the corresponding term to the frequency domain and computation of the spectral phase of one of the terms results in the spectral phase of the signal up to the known phase of the reference pulse and a linear phase contribution from the delay.

$$\Phi^{(+)}(\omega) = \arg\{\hat{S}^{(+)}(\omega)e^{j\omega\tau}\} = \varphi_S(\omega) - \varphi_R(\omega) + \omega\tau \tag{10.48}$$
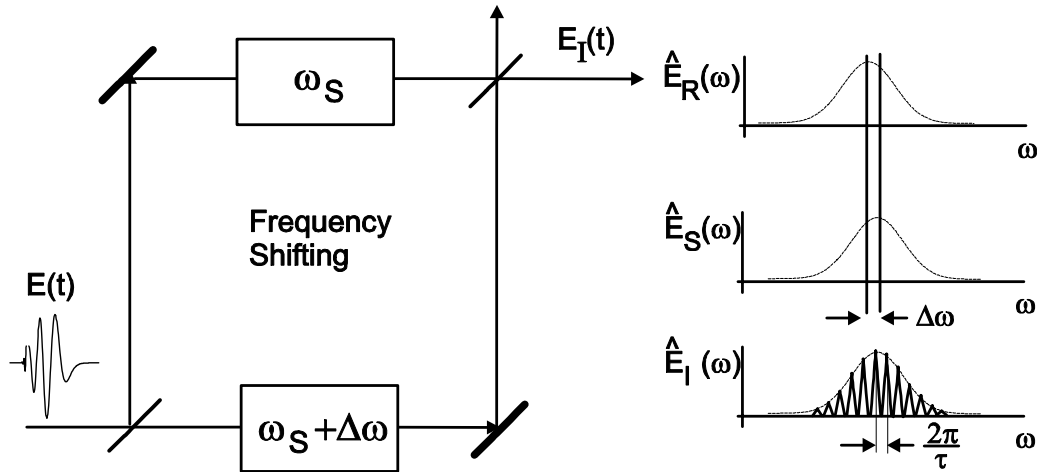
Figure 10.23: The principle of operation of SPIDER.

Adapted from F. X. Kaertner. *Few-Cycle Laser Pulse Generation and its Applications.* New York, NY: Springer-Verlag, 2004.

10.4.2 SPIDER

What can we do if we don't have a well characterized reference pulse? C. Iaconis and I.A. Walmsley [?] came up with the idea of generating two up-converted spectra slightly shifted in frequency and to investigate the spectral interference of these two copies, see Figure 10.23. We use

$$E_R(t) = E(t)e^{j\omega_S t} \tag{10.49}$$
$$E_S(t) = E(t-\tau)e^{j(\omega_S+\Omega)t} \tag{10.50}$$
$$E_I(t) = E_R(t) + E_S(t) \tag{10.51}$$

where ω_s and $\omega_s + \Omega$ are the two frequencies used for upconversion and Ω is called the spectral shear between the two pulses. $E(t)$ is the unknown electric field with spectrum

$$\hat{E}(\omega) = \left|\hat{E}(\omega)\right|e^{j\varphi(\omega)} \tag{10.52}$$

Spectral interferometry using these specially constructed signal and reference pulses results in

$$\hat{S}(\omega) = \left|\int_{-\infty}^{+\infty} E_I(t)e^{-j\omega t}dt\right|^2 = \hat{S}_{DC}(\omega)+\hat{S}^{(-)}(\omega)e^{j\omega\tau}+\hat{S}^{(+)}(\omega)e^{-j\omega\tau} \tag{10.53}$$

$$
\begin{aligned}
\hat{S}^{(+)}(\omega) &= \hat{E}_R^*(\omega)\hat{E}_S(\omega) = \hat{E}^*(\omega - \omega_s)\hat{E}(\omega - \omega_s - \Omega) & (10.54)\\
\hat{S}^{(-)}(\omega) &= \hat{S}^{(+)*}(\omega) & (10.55)
\end{aligned}
$$

The phase $\psi(\omega) = \arg[\hat{S}^{(+)}(\omega)e^{-j\omega\tau}]$ derived from the isolated positive spectral component is

$$
\psi(\omega) = \varphi(\omega - \omega_s - \Omega) - \varphi(\omega - \omega_s) - \omega\tau. \qquad (10.56)
$$

The linear phase $\omega\tau$ can be substracted off after independent determination of the time delay τ. It is obvious that the spectral shear Ω has to be small compared to the spectral bandwdith $\Delta\omega$ of the pulse, see Fig. 10.23. Then the phase difference in Eq.(10.56) is proportional to the group delay in the pulse, i.e.

$$
-\Omega\frac{d\varphi}{d\omega} = \psi(\omega), \qquad (10.57)
$$

or

$$
\varphi(\omega) = -\frac{1}{\Omega}\int_0^\omega \psi(\omega')d\omega'. \qquad (10.58)
$$

Note, an error $\Delta\tau$ in the calibration of the time delay τ results in an error in the chirp of the pulse

$$
\Delta\varphi(\omega) = -\frac{\omega^2}{2\Omega}\Delta\tau. \qquad (10.59)
$$

Thus it is important to chose a spectral shear Ω that is not too small. How small does it need to be? We essentially sample the phase with a sample spacing Ω. The Nyquist theorem states that we can uniquely resolve a pulse in the time domain if it is only nonzero over a length $[-T, T]$, where $T = \pi/\Omega$. On the other side the shear Ω has to be large enough so that the fringes in the spectrum can be resolved with the available spectrometer.

SPIDER Setup

We follow the work of Gallmann et al. [?] that can be used for characterization of pulses only a few optical cycles in duration. The setup is shown in Figure 10.24.
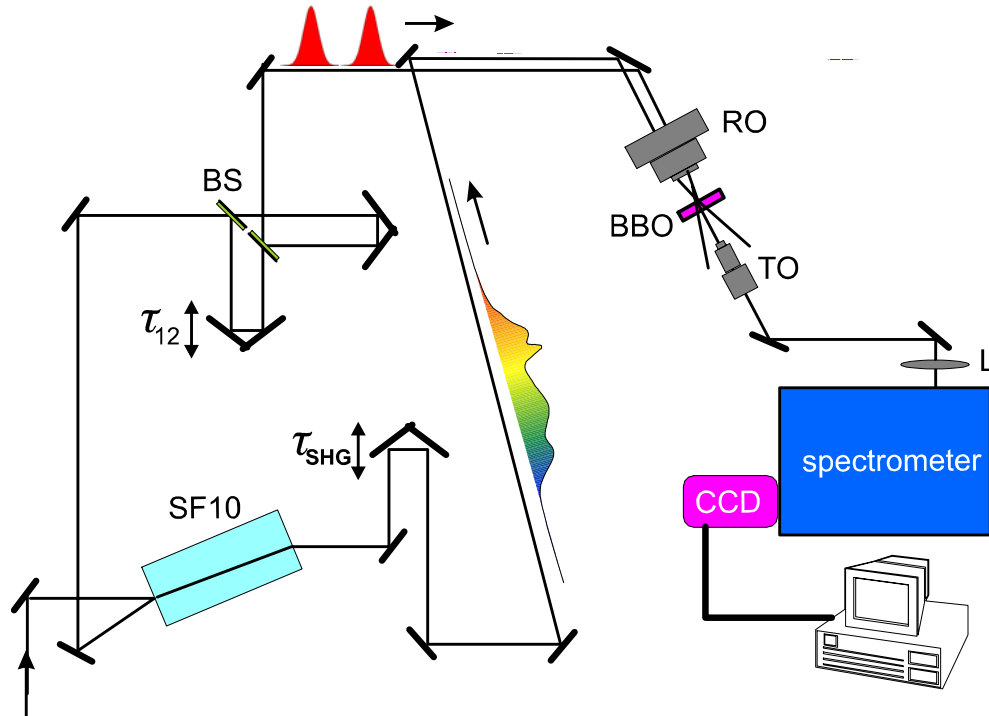

Figure 10.24: SPIDER setup; SF10: 65 mm glass block (GDD/z $\approx$ 160 fs^2/ mm), BS: metallic beam splitters ($\approx$ 200 μm, Cr–Ni coating 100 nm), τ: adjustable delay between the unchirped replica, τ_{SHG}: delay between unchirped pulses and strongly chirp pulse, RO: reflective objective (Ealing–Coherent, x35, NA=0.5, f=5.4 mm), TO: refractive objective , L: lens, spectrometer: Lot-Oriel MS260i, grating: 400 l/mm, Blaze–angle 350 nm, CCD: Andor DU420 CCI 010, 1024 x 255 pixels, 26 μm/pixel [13].

Courtesy of Richard Ell. Used with permission.

Generation of two replica without additional chirp:

A Michelson–type interferometer generates two unchirped replicas. The beam–splitters BS have to be broadband, not to distort the pulses. The delay τ between the two replica has to be properly chosen, i.e. in the setup shown it was about 400-500 fs corresponding to 120-150 μm distance in space.

Spectral shearing:

The spectrally sheared copies of the pulse are generated by sum-frequency generation (SFG) with quasi-monochromatic beams at frequencies ω_s and $\omega_s + \Omega$. These quasi monochromatic signals are generated by strong chirping of a third replica (cf. Fig. 10.24) of the signal pulse that propagates through a strongly dispersive glass slab. For the current setup we estimate for the broadening of a Gaussian pulse due to the glass dispersion from 5 fs to approximately 6 ps. Such a stretching of more than a factor of thousand assures that SFG occurs within an optical bandwidth less than 1 nm, a quasi–monochromatic signal. Adjustment of the temporal overlap τ_{SHG} with the two unchirped replica is possible by a second delay line. The streched pulse can be computed by propagation of the signal pulse $E(t)$ through the strongly dispersive medium with transfer characteristic

$$H_{glass}(\omega) = e^{-jD_{glass}(\omega-\omega_c)^2/2} \tag{10.60}$$

neglecting linear group delay and higher order dispersion terms. We otain for the analytic part of the electric field of the streched pulse leaving the glass block by convolution with the transfer characteristic

$$E_{stretch}(t) = \int_{-\infty}^{+\infty} \hat{E}(\omega)e^{-jD_{glass}(\omega-\omega_c)^2/2}e^{j\omega t}d\omega = \tag{10.61}$$

$$= e^{jt^2/(2D_{glass})}e^{j\omega_c t} \int_{-\infty}^{+\infty} \hat{E}(\omega)e^{-jD_{glass}((\omega-\omega_c)-t/D_{glass}{}^2)/2}d\omega \tag{10.62}$$

If the spectrum of the pulse is smooth enough, the stationary phase method can be applied for evaluation of the integral and we obtain

$$E_{stretch}(t) \propto e^{j\omega_c(t+t^2/(2D_{glass}))}\hat{E}(\omega = \omega_c + t/D_{glass}) \tag{10.63}$$

Thus the field strength at the position where the instantaneous frequency is

$$\omega_{inst} = \frac{d}{dt}\omega_c(t + t^2/(2D_{glass})) = \omega_c + t/D_{glass} \tag{10.64}$$

is given by the spectral amplitude at that frequency, $\hat{E}(\omega = \omega_c + t/D_{glass})$. For large stretching, i.e.

$$|\tau_p/D_{glass}| \ll |\Omega| \tag{10.65}$$

the up-conversion can be assumed to be quasi monochromatic.

SFG:

A BBO crystal (wedged 10–50 μm) is used for type I phase–matched SFG. Type II phase–matching would allow for higher acceptance bandwidths. The pulses are focused into the BBO–crystal by a reflective objective composed of curved mirrors. The signal is collimated by another objective. Due to SFG with the chirped pulse the spectral shear is related to the delay between both pulses, τ, determined by Eq.(10.64) to be

$$\Omega = -\tau/D_{glass}. \tag{10.66}$$

Note, that conditions (10.65) and (10.66) are consistent with the fact that the delay between the two pulses should be much larger than the pulse width τ_p which also enables the separation of the spectra in Fig.10.22 to determine the spectral phase using the Fourier transform method. For characterization of sub-10fs pulses a crystal thickness around 30 μm is a good compromise. Efficiency is still high enough for common cooled CCD–cameras, dispersion is already sufficiently low and the phase matching bandwidth large enough.

Signal detection and phase reconstruction:

An additional lens focuses the SPIDER signal into a spectrometer with a CCD camera at the exit plane. Data registration and analysis is performed with a computer. The initial search for a SPIDER signal is performed by chopping and Lock–In detection.The chopper wheel is placed in a way that the unchirped pulses are modulated by the external part of the wheel and the chirped pulse by the inner part of the wheel. Outer and inner part have different slit frequencies. A SPIDER signal is then modulated by the difference (and sum) frequency which is discriminated by the Lock–In amplifier. Once a signal is measured, further optimization can be obtained by improving the spatial and temporal overlap of the beams in the BBO–crystal.

One of the advantages of SPIDER is that only the missing phase information is extracted from the measured data. Due to the limited phase–matching bandwidth of the nonlinear crystal and the spectral response of grating and CCD, the fundamental spectrum is not imaged in its original form but rather with reduced intensity in the spectral wings. But as long as the interference fringes are visible any damping in the spectral wings and deformation of the spectrum does not impact the phase reconstruction process the SPIDER

technique delivers the correct information. The SPIDER trace is then generated by detecting the spectral interference of the pulses

$$
\begin{align}
E_R(t) &= E(t)\hat{E}(\omega_s)e^{j\omega_s t} \tag{10.67}\\
E_S(t) &= E(t-\tau)\hat{E}(\omega_s + \Omega)e^{j(\omega_s + \Omega)t} \tag{10.68}\\
E_I(t) &= E_R(t) + E_S(t) \tag{10.69}
\end{align}
$$

The positive and negative frequency components of the SIDER trace are then according to Eqs.(**??**,10.55)

$$
\begin{align}
\hat{S}^{(+)}(\omega) &= \hat{E}_R^*(\omega)\hat{E}_S(\omega) = \hat{E}^*(\omega - \omega_s)\hat{E}(\omega - \omega_s - \Omega)\hat{E}^*(\omega_s)\hat{E}(\omega_s + \Omega) \tag{10.70}\\
\hat{S}^{(-)}(\omega) &= \hat{S}^{(+)*}(\omega) \tag{10.71}
\end{align}
$$

and the phase $\psi(\omega) = \arg[\hat{S}^{(+)}(\omega)e^{-j\omega\tau}]$ derived from the isolated positive spectral component substraction already the linear phase off is

$$
\psi(\omega) = \varphi(\omega - \omega_s - \Omega) - \varphi(\omega - \omega_s) - \varphi(\omega - \omega_s - \Omega) + \varphi(\omega_s - \Omega) - \varphi(\omega_s). \tag{10.72}
$$

Thus up to an additional constant it delivers the group delay within the pulse to be characterized. A constant group delay is of no physical significance.

SPIDER–Calibration

This is the most critical part of the SPIDER measurement. There are three quantities to be determined with high accuracy and reproducibility:

- delay τ

- shift ω_s

- shear Ω

Delay τ:
The delay τ is the temporal shift between the unchirped pulses. It appears as a frequency dependent phase term in the SPIDER phase, Eqs. (10.56) and leads to an error in the pulse chirp if not properly substracted out, see Eq.(10.59).

A determination of τ should preferentially be done with the pulses detected by the spectrometer but without the spectral shear so that the observed fringes are all exactly spaced by $1/\tau$. Such an interferogram may

be obtained by blocking the chirped pulse and overlapping of the individual SHG signals from the two unchirped pulses. A Fourier transform of the interferogram delivers the desired delay τ.In practice, this technique might be difficult to use. Experiment and simulation show that already minor changes of τ (± 1 fs) significantly alter the reconstructed pulse duration ($\approx \pm 1 - 10\%$).

Another way for determination of τ is the following. As already mentioned, τ is accessible by a differentiation of the SPIDER phase with respect to ω. The delay τ therefore represents a constant GDD. An improper determination of τ is thus equivalent to a false GDD measurement. The real physical GDD of the pulse can be minimized by a simultaneous IAC measurement. Maximum signal level, respectively shortest IAC trace means an average GDD of zero. The pulse duration is then only limited by higher order dispersion not depending on τ. After the IAC measurement, the delay τ is chosen such that the SPIDER measurement provides the shortest pulse duration. This is justified because through the IAC we know that the pulse duration is only limited by higher order dispersion and not by the GDD $\propto \tau$. The disadvantage of this method is that an additional IAC setup is needed.
Shift ω_s:
The SFG process shifts the original spectrum by a frequency $\omega_s \approx 300$ THz towards higher frequencies equivalent to about 450 nm when Ti:sapphire pulses are characterized. If the SPIDER setup is well adjusted, the square of the SPIDER interferogram measured by the CCD is similar to the fundamental spectrum. A determination of the shift can be done by correlating both spectra with each other. Determination of ω_s only influences the frequency too which we assign a give phase value, which is not as critical.
Shear Ω:
The spectral shear is uncritical and can be estimated by the glass dispersion and the delay τ.

10.4.3 Characterization of Sub-Two-Cycle Ti:sapphire Laser Pulses

The setup and the data registration and processing can be optimized such that the SPIDER interferogram and the reconstructed phase, GDD and intensity envelope are displayed on a screen with update rates in the range of 0.5-1s.

Real–time SPIDER measurements enabled the optimization of external

dispersion compensation leading to 4.8 fs pulses directly from a laser [13], see Figure 10.25.
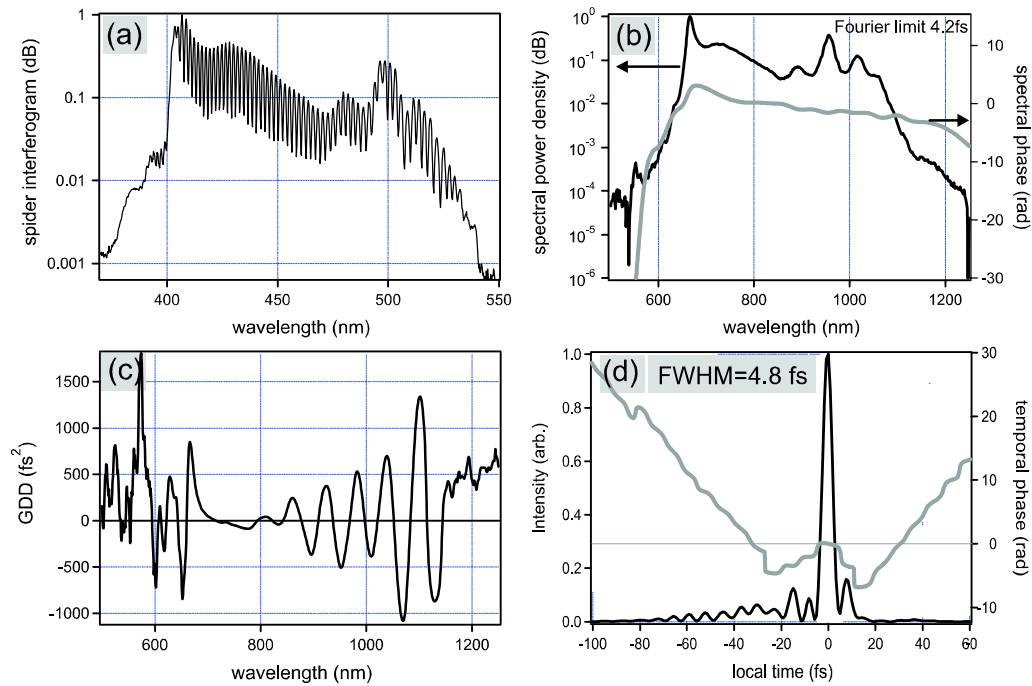

Figure 10.25: SPIDER measurement of a 4.8 fs Ti:sapphire laser pulse. (a) SPIDER interferogram on a logarithmic scale. (b) Spectral power density and spectral phase of the pulse. (c) Calculated GDD of the pulse. (d) Intensity envelope and temporal phase curve [13].

Courtesy of Richard Ell. Used with permission.

Figure 10.25(a) shows the SPIDER interferogram as detected by the CCD camera. The interferogram is modulated up to 90%, the resolutions limit in the displayed graphic can not resolve this. The large number of interference fringes assures reliable phase calculation. Figure (b) displays the laser spectrum registered by the optical spectrum analyzer on a logarithmic scale. The calculated spectral phase curve is added in this plot. The small slope of the phase curve corresponds to a constant GD which is an unimportant time shift. Fig. 10.25 (c) depicts the GDD obtained from the phase by two derivatives with respect to the angular frequency ω. The last Figure (d)

shows the intensity envelope with a FWHM pulse duration of 4.8 fs together with the temporal phase curve.

10.4.4   Pros and Cons of SPIDER

Advantages	Disadvantages
direct analytical phase extraction	complex experimental setup
no moving mirrors or other components	precise delay calibration necessary
possible real–time characterization	"compact" spectrum necessary
	(no zero-intensity intervals)
simple 1–D data acquisition	need for expensive CCD–camera
minor dependence on spectral response of nonlinear crystal and spectrometer	

Bibliography

[1] K. Naganuma, K. Mogi, H. Yamada, "General method for ultrashort light pulse chirp measurement," IEEE J. of Quant. Elec. **25**, 1225 - 1233 (1989).

[2] J. C. Diels, J. J. Fontaine, and F. Simoni, "Phase Sensitive Measurement of Femtosecond Laser Pulses From a Ring Cavity," in Proceedings of the International Conf. on Lasers. 1983, STS Press: McLean, VA, p. 348-355. J. C. Diels et al.,"Control and measurement of Ultrashort Pulse Shapes (in Amplitude and Phase) with Femtosecond Accuracy," Applied Optics **24**, 1270-82 (1985).

[3] J.W. Nicholson, J.Jasapara, W. Rudolph, F.G. Ometto and A.J. Taylor, "Full-field characterization of femtosecond pulses by spectrum and cross-correlation measurements, "Opt. Lett. **24**, 1774 (1999).

[4] D. T. Reid, et al., Opt. Lett. **22**, 233-235 (1997).

[5] R. Trebino, "Frequency-Resolved Optical Gating: the Measurement of Ultrashort Laser Pulses,"Kluwer Academic Press, Boston, (2000).

[6] Trebino, et al., Rev. Sci. Instr., 68, 3277 (1997).

[7] Kane and Trebino, Opt. Lett., 18, 823 (1993).

[8] Stark, Image Recovery, Academic Press, 1987.

[9] L. Cohen, "Time-frequency distributions-a review, " Proceedings of the IEEE, **77**, 941 - 981 (1989).

[10] L. Gallmann, D. H. Sutter, N. Matuschek, G. Steinmeyer and U. Keller, "Characterization of sub-6fs optical pulses with spectral phase interferometry for direct electric-field reconstruction," Opt. Lett. **24**, 1314 (1999).

[11] C. Iaconis and I. A. Walmsley, Self-Referencing Spectral Interferometry for Measuring Ultrashort Optical Pulses, IEEE J. of Quant. Elec. **35**, 501 (1999).

[12] C. Froehly, A. Lacourt, J. C. Vienot, "Notions de reponse impulsionelle et de fonction de tranfert temporelles des pupilles opticques, justifications experimentales et applications," Nouv. Rev. Optique 4, **18** (1973).

[13] Richard Ell, "Sub-Two Cycle Ti:sapphire Laser and Phase Sensitive Nonlinear Optics," PhD-Thesis, University of Karlsruhe (TH), (2003).